Single-Satellite Location of Ground Electromagnetic Interferer Exploiting Doppler Signatures

Yimin D. Zhang [1], Yanwu Ding [2], Khanh Pham [3], Dan Shen [4], and Genshe Chen [4]

[1] Department of Electrical and Computer Engineering, Temple University, Philadelphia, PA 19122, USA
[2] Department of Electrical and Computer Engineering, Wichita State University, Wichita, KS 67260, USA
[4] Air Force Research Laboratory, Kirtland Air Force Base, NM 87117, USA
[4] Intelligent Fusion Technology, Inc., Germantown, MD 20876, USA

***Abstract* —** We consider the single-satellite, single-pass localization of ground electromagnetic interference (EMI) sources to protect the quality of service in satellite communications. For a stationary EMI source, the analysis of the time-varying Doppler signature caused by satellite motion provides valuable information for its localization. Due to the high-speed motion of the satellite, the instantaneous Doppler frequency exhibits a high dynamic range and significant nonlinearity. To address this, we previously developed a knowledge-aided signal stationarization approach using the concept of virtual ground references (VGR), thereby enabling a reduced sampling rate, extended coherent processing time, and improved EMI detectability and accuracy. In this paper, we propose several extended approaches, including simplified multi-VGR data fusion as well as iterative and sequential EMI localization methods, to further enhance EMI localization performance while reducing processing complexity.

I. Introduction

Ground interference and spoofing signals pose significant threats to satellite communications and satellite-based navigation systems [1–4]. Accurate localization and effective suppression of these sources are critical steps toward mitigating their impact. When multiple synchronized satellites are available, ground emitters can be localized using methods based on time difference-of-arrival (TDOA) and frequency difference-of-arrival (FDOA) [5–7]. However, in scenarios where only a single satellite is available, locating ground interference sources becomes more challenging and often relies on analyzing Doppler signatures [8–10]. For a stationary ground electromagnetic interference (EMI) source, the high-speed orbital motion of the satellite generates a highly dynamic Doppler frequency, characterized as a nonlinear frequency-modulated (FM) signature [11].

This paper addresses the localization of a ground EMI source based on single-pass observations from a single satellite. The highly dynamic Doppler signatures typically require a high sampling rate and significant processing time for their analyses, and achieving a long coherent processing time poses additional challenges. To mitigate these issues, we previously developed a knowledge-aided approach [12]. This method involves coarsely stationarizing the Doppler signatures, followed by time-frequency analysis using the low-complexity short-time Fourier transform (STFT). Such stationarization is achieved by introducing a virtual ground reference (VGR) near the EMI source, leveraging the fact that coarse knowledge of the EMI source location is often available, for instance, through the directional beams used in satellite communication links [13, 14]. This processing effectively reduces the dynamic range and slope of the Doppler signatures, thereby extending the coherent processing time and enhancing EMI detectability and localization accuracy.

In this paper, we propose several extensions to these approaches to further enhance the EMI localization performance while reducing the processing complexity. The proposed enhancements include selecting the nearest VGR positions for multi-VGR data fusion, iterative processing by placing a single VGR at the previously estimated EMI position, and sequential EMI localization using EMI position estimates obtained from prior time instants.

Notations: Vectors are denoted using bold lower-case letters. $(\cdot)^{\mathrm{T}}$ and $\|.\|$ respectively represent the transpose and the Euclidean norms of a vector.

II. Signal Model

We consider the problem in a two-dimensional x-z coordinate for simplicity. Denote the location of the stationary EMI as vector $\boldsymbol{x}_e = [x_e, z_e]^{\mathrm{T}}$ and that of the satellite at time instant t as $\boldsymbol{x}_s(t) = [x_s(t), z_s(t)]^{\mathrm{T}}$. The instantaneous velocity vector of the satellite is denoted as $\boldsymbol{v}(t) = [v_x(t), v_z(t)]^{\mathrm{T}}$. The direction of $\boldsymbol{v}(t)$ varies over time as the satellite follows its elliptic orbit.

Denote the vector connecting the satellite and the EMI at time instant t as

$$\boldsymbol{r}_{es}(t) = \boldsymbol{x}_s(t) - \boldsymbol{x}_e, \tag{1}$$

and the corresponding distance as $D_{es}(t) = \|\boldsymbol{r}_{es}(t)\|$. The instantaneous Doppler frequency of a signal transmitted from

This material is based upon work supported by the Air Force Research Laboratory (AFRL) under Contract No. FA9453-22-C-A127. Any opinions, findings and conclusions or recommendations expressed in this material are those of the authors and do not necessarily reflect the views of the AFRL.

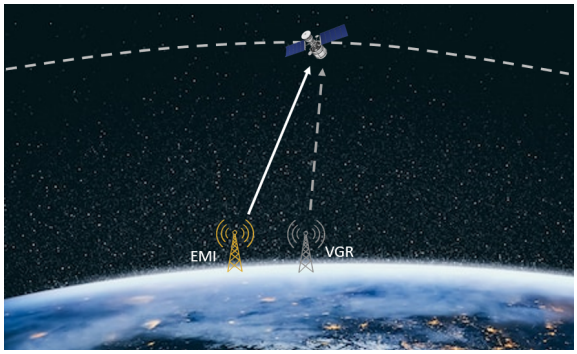

Fig. 1: Geometrical presentation of VGR-based approach.

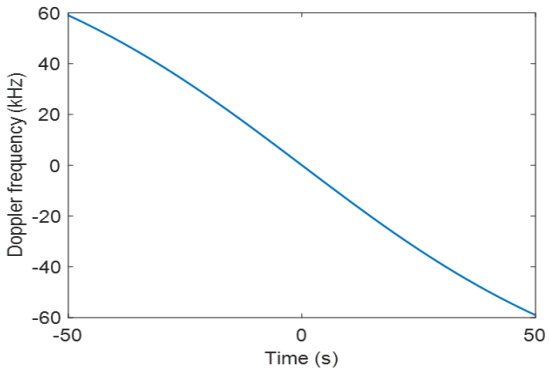

Fig. 2: Doppler signature of the EMI signal due to satellite motion.

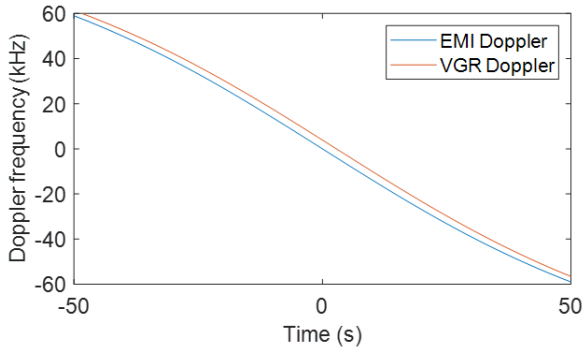

(a) Doppler frequencies of the EMI and VGR signals

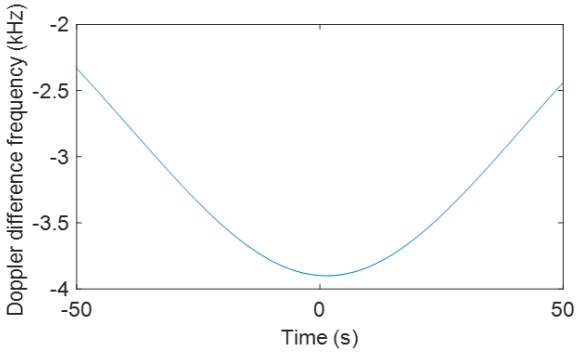

(b) Doppler difference frequency

Fig. 3: Doppler frequency and Doppler difference frequency ($x_v = 20$ km).

the ground EMI is expressed as

$$f_{D,es}(t) = -\frac{1}{\lambda} \cdot \frac{\mathrm{d}D_{es}(t)}{\mathrm{d}t} = -\frac{1}{\lambda}\boldsymbol{v}^{\mathrm{T}}(t)\bar{\boldsymbol{r}}_{es}(t), \tag{2}$$

where $\bar{\boldsymbol{r}}_{es}(t) = \boldsymbol{r}_{es}(t)/\|\boldsymbol{r}_{es}(t)\|$ denotes the unit vector in the direction of $\boldsymbol{r}_{es}(t)$.

Due to the high speed of the satellite, the Doppler frequency is characterized as a highly nonlinear FM signature. For the parameters shown in Table 1, Fig. 2 illustrates the Doppler frequency observed over a 100-second period between -50 sec $\leq t \leq 50$ sec. The Doppler frequency changes at different rates depending on the satellite's position.

Table 1. Parameters Used in the Simulations

Parameter	**Value**
Satellite altitude	600 km
Satellite speed	7,800 m/s
Carrier frequency	4.5 GHz
EMI position	$[0, 0, 0]^{\mathrm{T}}$ km

III. VGR-Based EMI Localization

VGR-based EMI localization utilizes knowledge-aided quasi-stationarization processing, which aims to reduce the dynamic range and slope of the Doppler signatures. The beamforming capability of the satellite provides coarse information about the EMI, which can be used to determine VGR locations in the vicinity of the EMI. Similar to the EMI case, the Doppler frequency corresponding to a VGR $\boldsymbol{x}_i = [x_i, z_i]^{\mathrm{T}}$ is given by

$$f_{D,is}(t) = -\frac{1}{\lambda}\boldsymbol{v}^{\mathrm{T}}(t)\bar{\boldsymbol{r}}_{is}(t), \tag{3}$$

where $\boldsymbol{r}_{is}(t) = \boldsymbol{x}_s(t) - \boldsymbol{x}_i$ and $\bar{\boldsymbol{r}}_{is}(t) = \boldsymbol{r}_{is}(t)/\|\bar{\boldsymbol{r}}_{is}(t)\|$.

We compute the Doppler difference between $f_{D,es}(t)$ and $f_{D,is}(t)$ as

$$\begin{aligned}\Delta f_{D,i}(t) &= f_{D,es}(t) - f_{D,is}(t) \\ &= -\frac{1}{\lambda}\boldsymbol{v}^{\mathrm{T}}(t)[\bar{\boldsymbol{r}}_{es}(t) - \bar{\boldsymbol{r}}_{is}(t)] \approx \frac{1}{\lambda}\frac{\boldsymbol{v}^{\mathrm{T}}(t)\boldsymbol{r}_{ei}}{\|\boldsymbol{r}_{is}(t)\|},\end{aligned} \tag{4}$$

where $\boldsymbol{r}_{ei}$ is a vector connecting the EMI and the ith VGR. The last approximation in the above expression is obtained by assuming $\|\boldsymbol{r}_{vs}(t)\| \approx \|\boldsymbol{r}_{is}(t)\|$. Because $\|\boldsymbol{r}_{ei}\|$ is much smaller than $\|\boldsymbol{r}_{is}(t)\|$, the value of $|\Delta f_{D,i}(t)|$ is much smaller than $|f_{D,es}(t)|$, thus reducing both the dynamic range and slope of the Doppler difference compared to those of the original Doppler signatures.

Consider an example where a VGR is placed at $x_v = 20$ km. In this case, the Doppler signatures corresponding to

the EMI and the VGR are compared in Fig. 3(a), and the Doppler difference between them is shown in Fig. 3(b). These two Doppler frequencies are close and vary in a similar manner, and the resulting Doppler difference changes much more slowly with a small dynamic range. Such results enable processing the data at a reduced sampling rate and exploiting a longer window size when computing the STFT. In [12], it is shown that integrating the magnitude of the STFT over a time period between 10 and 11 seconds results in a peak indicating the value of the Doppler difference. An example of the spectrogram is shown in Fig. 4(a), and the integrated magnitude, showing in Fig. 4(b), clearly indicates a peak at a Doppler difference of $\Delta\hat{f}_{D,i}(t) = -3,896.48$ Hz.

Based on such an estimate using a single VGR, the EMI location can be estimated using the following expression at a specific time instant t:

$$\hat{x}_e(t) \approx x_i + \frac{\lambda \cdot \|\boldsymbol{r}_{is}(t)\|}{v_x} \Delta\hat{f}_{D,i}(t). \tag{5}$$

For the example showing in Fig. 4(b), the EMI position is estimated as $\hat{x}_e = -59.4$ m, which is very close to the true EMI source position at $x_e = 0$ m.

IV. Multi-VGR EMI Localization

It is clear that, when a VGR is chosen to be closer to the true EMI location, the Doppler difference becomes smaller, resulting in better energy concentration in the STFT results. In the extreme case, when the VGR coincides with the true EMI location, the Doppler difference $|\Delta f_{D,i}(t)| = 0$ becomes time-invariant.

In Fig. 5, the red vertical lines, from left to right, show the true Doppler differences for different VGR positions, varying from 80 km to -80 km in 10-km steps. The circles and dots together represent the estimated Doppler differences and the corresponding peak values from a single random realization, when the STFT magnitude is of interest between 10 and 11 seconds. For clarity, we also list the values in Table 2. When the VGR positions are -80, -70, -60, and -50 km, meaningful peak values are not detected. Note that the results are not symmetric because the satellite, during this time period, has a positive x location, which favors VGR positions in the positive range of the x values.

Because the true EMI position is unknown, we need to try this process for multiple locations in the vicinity of the anticipated EMI position. Repeating this process over a large number of VGR positions introduces high complexity. As such, only a small number of VGRs are used. In [12], several VGR positions are selected, and the estimated EMI positions from different VGRs are averaged using a softmax weight.

V. Improved EMI Localization Methods

In this paper, we improve the EMI localization through the following three approaches.

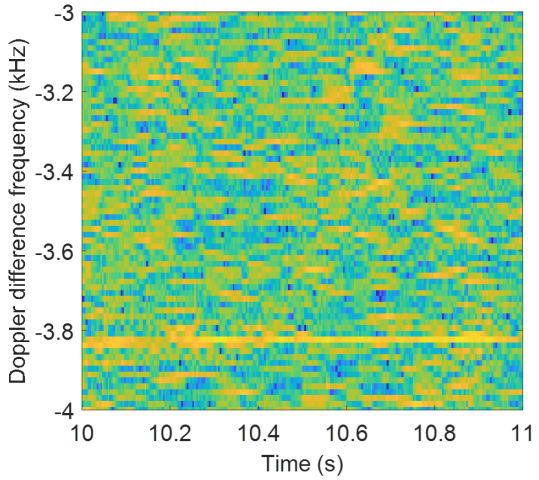

(a) Doppler frequencies of the EMI and VGR signals

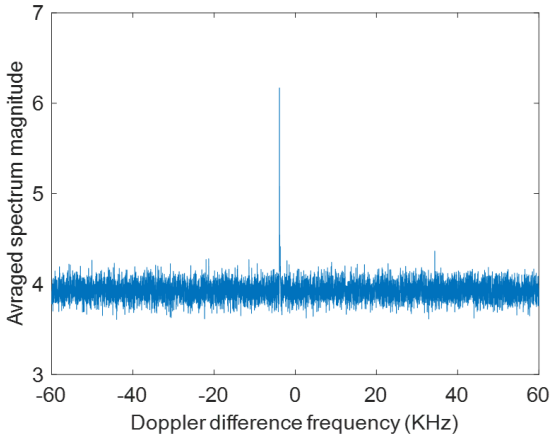

(b) Doppler difference frequency

Fig. 4: Doppler frequency and Doppler difference frequency ($x_v = 20$ km).

A. Simplified Multi-VGR Data Fusion

Notice that the Doppler difference has a high accuracy and takes positive and negative values depending on their locations relative to the true EMI. Therefore, we can easily choose the two Doppler difference values that are closest to 0 respectively with positive and negative Doppler differences. The EMI would lie between these VGR positions and weighted averaging over these two results would eliminate the effect of other noisy results.

As an example, we consider six VGR positions at $x_i = -80, -50, -20, 10, 40, 70$ km. Note that we choose the VGR locations to be asymmetric so as not to take advantages of the coarse symmetry of the results as the exact EMI position is unknown. In this case, as depicted in Fig. 5 and Table 2, we can identify such two VGR positions closest to the EMI with opposite relative positions are $x_i = -20$ km and 10 km. The EMI positions estimated using Eq. (5) based on these Doppler

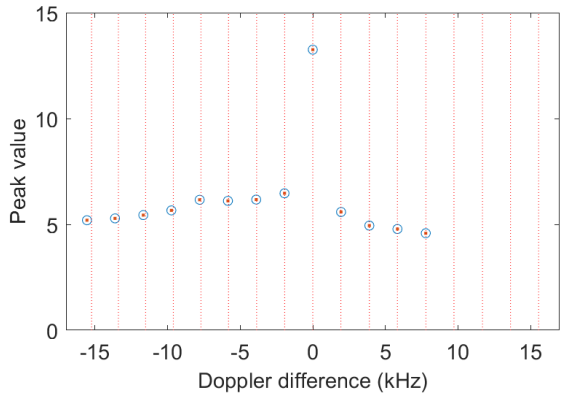

Fig. 5: Estimated Doppler frequency and peak values corresponding to different VGR positions.

Table 2. Estimated Doppler difference values

VGR Position (km)	True Doppler Difference (kHz)	Est. Doppler Difference (kHz)	Peak Value
-80	15.5566		
-70	13.6230		
-60	11.6895		
-50	9.7266		
-40	7.7930	7.7832	4.5803
-30	5.8301	5.8301	4.7815
-20	3.8965	3.8965	4.9422
-10	1.9336	1.9482	5.5849
0	0.0000	0.0000	13.2516
10	-1.9359	-1.9482	6.4660
20	-3.8672	-3.8965	6.1706
30	-5.8008	-5.8447	6.1102
40	-7.7051	-7.7930	6.1611
50	-9.6094	-9.7412	5.6604
60	-11.5137	-11.6748	5.4382
70	-13.3887	-13.6230	5.2821
80	-15.2334	-15.5566	5.1953

difference estimates are respectively 231.16 m and -47.10 m. Applying the softmax weights [12] to only these two VGR positions yields an estimated EMI position of -47.10 m.

B. Iterative EMI Localization

With the EMI position estimated from the previous step, we can further enhance the estimation by placing a single VGR at this estimated EMI position. Compared to the sparsely distributed VGRs initially chosen, the estimated EMI provides much better VGR placement for improved EMI localization.

By placing a VGR at -47.10 m, we find that the EMI position is estimated as $\hat{x}_e = 28.59$ m. In this case, the residual estimation error is due to the resolution in the Doppler difference analysis.

C. Sequential EMI Localization

It is noted that the above results are obtained from one time segment, where a one-second period between 10 second and 11 second is used for the simulations. It is straightforward to apply the result forward to the next processing interval, say, a one-second period between 11 second and 12 second is used for the simulations. As such, we only need to use a single VGR, placed at the previous estimated EMI position of $\hat{x}_e = 28.59$ m, to achieve a high accuracy. In this case, the EMI position in the new time period is estimated as $\hat{x}_e = 26.96$ m.

VI. Conclusion

In this paper, we considered the EMI localization using a single satellite. It extended the previous work which exploits Doppler difference between the EMI signals and that of VGRs placed in the vicinity of the EMI based on the coarse information of the EMI. The modifications and extensions made in this paper include the selection of closest VGR positions for multi-VGR data fusion, iterative processing by placing a single VGR at the previously estimated EMI position, and sequential EMI localization using estimated EMI position from previous time instants. These methods collectively achieve enhanced EMI localization with reduced complexity.

References

[1] S. K. Sharma, S. Chatzinotas, and B. Ottersten, "Satellite cognitive communications: Interference modeling and techniques selection," in *Proceedings of Advanced Satellite Multimedia Systems Conference and Signal Processing for Space Communications Workshop*, 2012, pp. 111–118.

[2] Y. D. Zhang and M. G. Amin, "Anti-jamming GPS receiver with reduced phase distortions," *IEEE Signal Processing Letters*, vol. 19, no. 10, pp. 635–638, 2012.

[3] M. L. Psiaki and T. E. Humphreys, "GNSS spoofing and detection," *Proceedings of the IEEE*, vol. 104, no. 6, pp. 1258–1270, 2016.

[4] T. J. O'Shea, R. W. McGwier, and N. A. McCarthy, "Apparatuses, systems and methods for obtaining information about electromagnetic energy emitted from the earth, such as for locating an interference source on earth," May 2017, US Patent S 9,661,604.

[5] T. Pattison and S. Chou, "Sensitivity analysis of dual-satellite geolocation," *IEEE Transactions on Aerospace and Electronic Systems*, vol. 36, no. 1, pp. 56–71, 2000.

[6] K. Ho and W. Xu, "An accurate algebraic solution for moving source location using TDOA and FDOA measurements," *IEEE Transactions on Signal Processing*, vol. 52, no. 9, pp. 2453–2463, 2004.

[7] D. Musicki, R. Kaune, and W. Koch, "Mobile emitter geolocation and tracking using TDOA and FDOA

measurements," *IEEE Transactions on Signal Processing*, vol. 58, no. 3, pp. 1863–1874, 2010.

[8] P. Ellis, D. V. Rheeden, and F. Dowla, "Use of Doppler and Doppler rate for RF geolocation using a single LEO satellite," *IEEE Access*, vol. 8, pp. 12 907–12 920, 2020.

[9] D. Shen, G. Chen, and K. Pham, "Passive single satellite geolocation of ground-based EMI sources," in *Proceedings of ION GNSS+*, Denver, CO, Sept. 2023, pp. 2384–2394.

[10] Y. Ding, C. Minkler, Y. D. Zhang, D. Shen, and K. Pham, "Single-satellite EMI geolocation via flexibly constrained UKF exploiting Doppler acceleration," *IEEE Signal Processing Letters*, in press.

[11] C.-C. Sun and S.-S. Jan, "Time-frequency analyses of global navigation satellite system signals," in *Proceedings of ION GNSS*, 2009, pp. 2629–2636.

[12] Y. D. Zhang, Y. Ding, K. P. amd Dan Shen, and G. Chen, "Doppler-based satellite-borne localization of ground electromagnetic interferer," in *Proceedings of IEEE Aerospace Conference*, Big Sky, MT, March 2024.

[13] M. A. Vázquez, A. Pérez-Neira, D. Christopoulos, S. Chatzinotas, B. Ottersten, P.-D. Arapoglou, A. Ginesi, and G. Taricco, "Precoding in multibeam satellite communications: Present and future challenges," *IEEE Wireless Communications*, vol. 23, no. 6, pp. 88–95, 2016.

[14] Y. D. Zhang and K. D. Pham, "Joint precoding and scheduling optimization in downlink multicell satellite communications," in *Proceedings of Asilomar Conference on Signals, Systems, and Computers*, Pacific Grove, CA, Nov. 2020, pp. 480–484.